

AD-A094 271

ILLINOIS UNIV AT URBANA-CHAMPAIGN DEPT OF METALLURGY --ETC F/G 11/6
HYDROGEN EFFECTS IN NICKEL-EMBRITTLMENT OR ENHANCED DUCTILITY.(U)
NOV 80 J EASTMAN, T MATSUMOTO, N NARITA N00014-75-C-1012

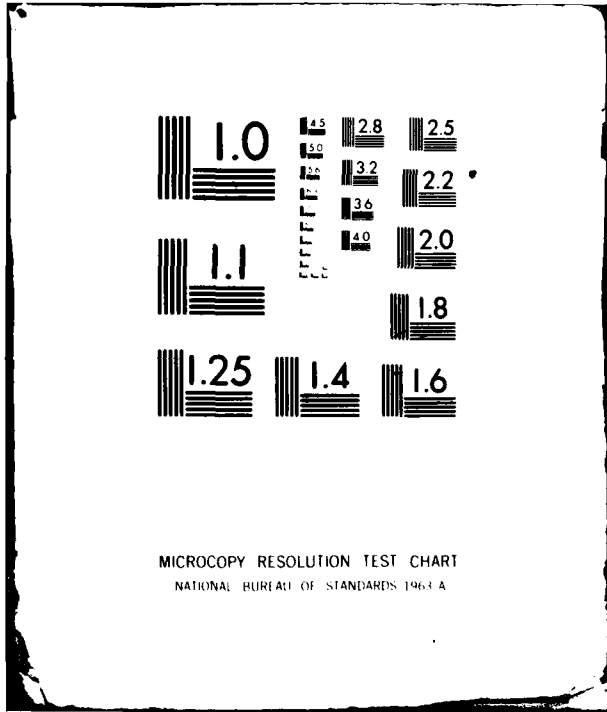
UNCLASSIFIED

NL

1-1
2-1
3-1



END
DATE
FILMED
2 81
DTIC



MICROCOPY RESOLUTION TEST CHART
NATIONAL BUREAU OF STANDARDS 1963-A

AD A094271

10
B 2

HYDROGEN EFFECTS IN NICKEL-EMBRITTLMENT
OR ENHANCED DUCTILITY

J. Eastman, T. Matsumoto, N. Narita, F. Heubaum
and H. K. Birnbaum

University of Illinois
Department of Metallurgy and Mining Engineering
Urbana, IL 61801

Technical Report

November 1980

W 00014-75-C-1012

DTIC
ELECTE

JAN 29 1981

A

This document is unclassified. Reproduction and distribution for any purpose of the U.S. Government is permitted.

DDC FILE COPY

This document has been approved
for release under the
Executive Order 11652

80 12 04 03

HYDROGEN EFFECTS IN NICKEL -- EMBRITTLEMENT OR ENHANCED DUCTILITY?

J. Eastman, T. Matsumoto, N. Narita, F. Heubaum and
H.K. Birnbaum

Department of Metallurgy and Mining Engineering
University of Illinois at Urbana-Champaign
Urbana, Illinois 61801

In the present work we have attempted to study hydrogen-related fracture of nickel using a variety of experimental methods with the principle aim of establishing the mechanism of fracture. Fracture of nickel was studied in low pressure hydrogen gas and for specimens containing solute hydrogen using slow strain rate tension tests. Both intergranular and transgranular fracture was observed on testing in hydrogen gas depending on the heat treatment and on the presence of trace impurities such as S, Mn, and Mg. The intergranular fracture mode was correlated with the segregation of S to the grain boundaries as measured by Auger and SIMS techniques. Specimens containing solute hydrogen fractured in an intergranular mode for all heat treatments. Detailed examination of both the intergranular and transgranular fracture surfaces indicated that neither was a truly "brittle" fracture mode but that both indicated a high degree of local ductility.

The effect of hydrogen on the plastic properties of nickel was examined using stress strain techniques and in situ deformation in an environmental cell in the HVEM. It was shown that hydrogen decreases the flow stress of nickel. In situ environmental cell fracture studies in hydrogen gas in the HVEM showed that the fracture process resulted from locally enhanced deformation at the crack tip due to the presence of hydrogen. This was confirmed by in situ fracture studies in the SEM.

Attch on file

page - A -

A

I. Introduction

Embrittlement of nickel and its alloys by solute and gaseous hydrogen is well established and has been extensively studied. Polycrystalline nickel has been reported to fracture in a brittle intergranular (IG) mode when charged with hydrogen (1-3) while single crystals containing solute hydrogen fail in a completely ductile mode (3). Kamdar (4) has recently reported that single crystals of nickel fracture in a transgranular (TG) mode when tested in gaseous H_2 . Both single and polycrystalline Ni specimens exhibit extensive plasticity prior to fracture so the process can hardly be considered a completely brittle one. Hydrogen effects have also been noted on the plastic response of nickel with solute strengthening and Portevin-Le Chatalier effects (5).

The mechanisms of the hydrogen-related fracture have not been established nor has it even been shown that the process is a brittle one. In the present paper we will summarize a series of experiments carried out at the University of Illinois which bear on the question of what determines the fracture path and what the fracture mechanism is. While a detailed discussion of mechanisms will be published elsewhere we will show in this paper that the fracture is largely a result of localized plastic processes which hydrogen assisted.

II. Experimental Procedures

A variety of alloys of Ni were prepared to study the effects of trace elements on the fracture and deformation behavior. In the present paper we shall review the results obtained for the alloys specified in Table I. Since the fracture behavior was noted to be extremely sensitive to the S distribution, several classes of heat treatments will be discussed:

Series VR; anneal at 1573K in a vacuum of 1.3×10^{-3} Pa followed by a 200K/sec quench into silicone oil;

Series VS, anneal at 1573K in a vacuum of 1.3×10^{-3} Pa, quench into silicone oil, age at 1173K for 3.6Ksec, followed by cooling at a rate of 0.03K/sec;

Series HR; same as VR above except the annealing and quench took place in 10^2 KPa of H_2 gas which introduced solute H at the level of 700 at.ppm. (Specimens were stored at 77K until used;

Series CR; same as VR above except the anneals and quenching took place in CO/CO₂ mixtures which were controlled to adjust the resulting C concentration;

Series CS; same as VS above except CO/CO₂ mixtures were used as annealing atmospheres.

Various specimen configurations including single crystals and relatively large grained polycrystals were used as required by the tests and these will be described in detail elsewhere. Tensile testing was carried out at strain rates of about 2×10^{-5} sec⁻¹ (or as subsequently specified) in 10^2 KPa H_2 atmospheres, vacuum, helium or air as required.

Table I. Concentrations* of Significant Alloying Elements in the Alloys Studied

Alloy/Heat Treatment	C	S	H	Mg	Mn
HP/VR	3200	44	0	0	0
HP/VS	3200	44	0	0	0
HP/CR	140	1.6	0	0	0
HP/CS	140	1.6	0	0	0
Cl/VR			0	2500	900
Cl/VS			0	2500	900
C2/HR	280	< 1	700	70	< 1
C3/CS					

* Atomic ppm; metallic elements by spark source mass spectroscopy, interstitials by vacuum fusion.

III. Results

A. Fracture Path

The results of fracture studies on polycrystalline specimens are shown in Table II where the values listed are the averages over many tests. After fracture detailed Auger analysis and depth profiling was carried out on the IG fracture facets and on the TG surfaces. The results of the Auger analysis clearly showed: (a) a high level of sulfur segregation on the IG fracture surfaces of specimens HP/VS and HP/CS; (b) no significant sulfur segregation on the IG fracture surfaces of specimens HP/VR, HP/CR or Cl/VR or Cl/VS; (c) no significant sulfur segregation at any of the TG fracture surfaces; (d) no significant sulfur segregation at the IG fracture surfaces at specimens C2/HR; (e) no elements other than sulfur exhibited any significant segregation at the fracture surfaces.

The extent of hydrogen embrittlement by gaseous H₂ or solute H₂ is clearly shown by the data of Table II. After a detailed analysis of the results (to be shortly published) we conclude the following:

- (a) The fracture path in specimens containing solute hydrogen (C2/HR) is IG over the temperature range 300-123K and since these specimens do not have S segregation at grain boundaries the IG fracture does not depend on S segregation. This result is consistent with that reported for fatigue fracture of Ni (6). Nickel specimens containing solute hydrogen exhibit IG fracture even when tested in 10² KPa of H₂. The IG fracture is observed even at temperatures (123K) where H diffusion is very slow and hydrogen diffusion to the fracture tip can not take place.
- (b) The fracture mode of Ni tested in gaseous H₂ atmospheres depends on the distribution of S in contrast to the behavior of specimens containing solute hydrogen. Specimens treated to segregate S at grain boundaries exhibit predominantly IG fracture (HP/VS, HP/CS) while in the absence of S segregation TG fracture is observed (HP/VS, HP/CR). The strain to failure is significantly less when the fracture mode is IG.

- (c) The presence of Mg and Mn in solid solution serve to trap the S and prevent segregation at grain boundaries. In these alloys (C1/VR, C1/VS) predominantly TG fracture is observed even in specimens (C1/VS) given an anneal which would cause S segregation and IG failure in the absence of Mg and Mn.
- (d) At the level of C concentrations used in the present experiments no significant effects are noted on the ductility of Ni specimens in the absence of H. When tested in gaseous H₂ the high C alloys (HP/VR, HP/VS) exhibited less ductility loss than the low C alloys (HP/CR, HP/CS).
- (e) The difference in energy between the IG and TG fracture paths must be relatively small as the fracture surface contains elements of both paths in all cases.
- (f) In all specimens testing in air or inert gases resulted in a completely ductile behavior with failure by microvoid coalescence. Sulfur segregation in the absence of solute H or gaseous H₂ had no effect on the fracture at the concentration levels of the present experiments.
- (g) The TG fracture surfaces had surface intersections which were parallel to the {111} slip plane traces. By carrying out two surface analyses of the fracture planes of single crystals tested in gaseous hydrogen the fracture plane was determined to be the {111}. This contrasts to the previous report of fracture along the {110} (7).

Table II. Fracture Characteristics

Alloy/ Heat Treatment	Test Atmosphere	% Reduction in Area	Fracture Mode
HP/VR	H ₂	75	20% IG 80% TG
	Air	95	Ductile Microvoid
HP/VS	H ₂	35	70% IG 30% TG
	Air	90	Ductile Microvoid
HP/CR	H ₂	55	20% IG 80% TG
	Air	95	Ductile Microvoid
HP/CS	H ₂	14	80% IG 20% TG
	Air	95	Ductile Microvoid
C1/VR	H ₂	55	25% IG 75% TG
	Air	90	Ductile Microvoid
C1/VS	H ₂	60	20% IG 80% TG
	Air	90	Ductile Microvoid
C2/HR	Vac.	26	~ 100% IG
	H ₂		~ 100% IG

B. Fractography

A large number of interesting features were noted on the fracture surfaces using high resolution SEM methods and these will be discussed in subsequent publications. At the present time we will focus on the generic features. Both IG and TG fracture surfaces were not truly "brittle" but showed many features characteristic of a high degree of local plasticity. The IG fracture surfaces obtained in specimens containing solute H or fractured in gaseous H_2 were qualitatively the same. There were no evident features which could be ascribed to the segregation of S at the grain boundaries.

Some features of the $\{111\}$ TG fracture surfaces are shown in Fig. 1. Traces of intersecting $\{111\}$ slip lines were observed (Figs. 1a and 1c) as were small hillocks and depressions, the sides of which appeared to correspond to the intersecting $\{111\}$ (Figs. 1c and 1d). No evidence for microvoids were observed in contrast to a previous report (7) (Fig. 1b). Secondary cracking was often observed (Figs. 1e and 1f). TG cracking in polycrystalline specimens showed many of the same features (Figs. 1f, 1g and 1h) but since the $\{111\}$ fracture plane was less well aligned with the tensile axis, the TG surfaces were often more highly stepped. The surfaces shown in Fig. 1 are clearly not the result of a true cleavage process (they are of the type often designated as "quasi-cleavage") and give the impression of a high degree of local plasticity. Identifiable "river lines" are observed but are significantly less sharply defined than in true cleavage.

Similar conclusions may be drawn from the IG fracture surfaces as shown in Fig. 2. Slip line markings (Fig. 2a) are observed as are patches of highly deformed regions (Fig. 2b). Rarely is the grain boundary surface revealed by IG fracture smooth and planar as would be expected if the fracture were due to "decohesion" along the boundary. The IG fractographs shown in Fig. 2 are typical of those produced by solute and by gaseous hydrogen.

C. In-situ Fracture Studies

The course of fracture was studied using in-situ SEM and HVEM fracture studies. SEM photographs of the tips of propagating cracks for Ni-H alloys are shown in Fig. 3. Studies of the video tapes of IG fractures clearly show the occurrence of a large amount of slip in both grains which is manifested in the large COD's shown in Figs. 3a-3c. Appreciable shear across the grain boundary often occurred in front of the crack tip (Fig. 3c). The crack would often proceed rapidly along a grain boundary until it intersected a triple point at which it would stop until sufficient grain boundary shear occurred in one of the boundaries in front of the crack tip. In many cases a new crack would open along the grain boundary in front of the main crack and then the two would grow together (Fig. 3a).

Similar SEM experiments were carried out in H_2 gas to produce TG fracture as shown in Fig. 3d. Large amounts of slip can be seen at the surface, some of which is due to the deformation obtained before the fracture began. Again there clearly is a good deal of plasticity accompanying the crack propagation as evidenced by the COD. No evidence for microvoid formation was seen.

A more detailed study of the TG crack tip processes was carried out using a tensile stage in an atmosphere of about 10^{-4} Pa H_2 gas in the HVEM and will be published in detail shortly. Some of the results are shown in Fig. 4. The tip of a fracture occurring in vacuum is shown in Figs. 4a and 4b which show a noncrystallographic fracture with a large

deformation zone and "holes" opening up in front of the main crack. This corresponds to the formation of microvoids. In contrast to this the crack tip and fracture surface in H_2 gas is highly crystallographic (Figs. 4c and 4d) with the fracture planes parallel to the $\{111\}$ as observed in macroscopic specimens. An extremely high dislocation density forms in front of the crack tip (Figs. 4e and 4f) and is observed all along the crack surfaces (Fig. 4g). The deformation is very highly localized along the $\{111\}$ slip planes in front of the crack tip rather than being broadly distributed. Examination of the video tapes shows that the fracture results from this localized deformation by a shearing of one-half of the crystal relative to the other. This fracture by slip on $\{111\}$ results in a thinned region along the fracture surface which is bounded by $\{111\}$ plane intersections as shown in Fig. 4d.

While the detailed relationships between the HVEM results and the fracture of macroscopic specimens cannot be discussed in detail, it is clear that both are the result of highly localized plastic processes which occur in the presence of H solutes or H_2 gas. A detailed correspondence between the fracture details is not expected due to differences in stress states but the sawtooth $\{111\}$ fractures (Figs. 4d and 4h) may correspond to the features shown in Figs. 1c and 1d. The results strongly suggest that slip is enhanced by the presence of hydrogen.

D. Hydrogen Effects on Plastic Deformation

Since the fracture process is closely related to a localized plasticity induced by hydrogen we examined this question using HVEM and tensile testing techniques the results of which will be reviewed. Plastic deformation in the HVEM in vacuum resulted in dislocation motion and generation as expected (Fig. 5a). The specimen displacement was held constant and H_2 gas was admitted to the environmental chamber. At about 10^3 Pa of H_2 dislocations were observed to begin to move and at about 10^4 Pa of H_2 rapid dislocation generation and motion occurred resulting in the structure shown in Fig. 5b. Similar experiments using He gas had no effect on the dislocation structure and since the specimen which was held at a constant displacement experienced a decreasing stress due to the dislocation motion, we conclude that the dislocation generation and motion was due to H introduced as a solute from the gas phase.

As a further demonstration of solute softening due to H, low strain rate tensile tests of 25 μm sheet specimens were carried out in 10^2 KPa of H_2 and He gas atmospheres with the typical results shown in Fig. 6. At high strain rates, $\dot{\epsilon} = 7 \times 10^{-5} \text{ sec}^{-1}$, the stress strain curves are identical for He and H_2 atmospheres. In contrast, slower strain rates, such as $\dot{\epsilon} = 10^{-7} \text{ sec}^{-1}$, showed lower flow stresses for specimens tested in H_2 as compared to those tested in He gas. This softening is observed in the microstrain range and in the post yield region. At higher strains the softening effect due to H_2 is reduced.

The cause of this decrease in flow stress due to H_2 is not yet established but it has the general characteristics of that observed on electrolytically charging Fe with H during deformation (8). We have measured the activation volume, $V^* = (RT)^{-1} \partial \ln \sigma / \partial \dot{\epsilon}$, and found no difference between the two atmospheres. One significant difference is the "internal stress"

as measured by the "stress dip test". Specimens deformed in He exhibited $\sigma_{int}/\sigma_{flow} \approx 0.85$ independent of the ϵ as expected for fcc metals. In contrast, deformation in H_2 gas resulted in $\sigma_{int}/\sigma_{flow} \approx 0.65$ at $\epsilon = 10^{-3}$ which increased to 0.85 at about $\epsilon \approx 3.5 \times 10^{-3}$. The lower σ_{int} for H_2 atmospheres is consistent with a marked difference in the dislocation structure as observed in the HVEM experiments and the increase in σ_{int} is also consistent with H enhanced plasticity. Thus, while the mechanisms are not well understood, it appears that small concentrations of H in solid solution have a major effect on enhancing dislocation motion.

IV. Conclusions

While only a brief summary of our results have been presented we can draw the following conclusions concerning hydrogen related fracture of Ni:

- (a) IG fracture of Ni in H_2 gas occurs when S segregation exists at grain boundaries. In the absence of S segregation a TG mode is observed.
- (b) IG fracture of Ni containing solute hydrogen occurs whether or not S segregation at grain boundaries occurs.
- (c) Mg and Mn can act as traps for S to prevent segregation at the grain boundaries.
- (d) The IG and TG fracture processes result from a localized deformation process at the crack tip. The importance of H enhanced plastic processes at crack tips was first suggested for steels by Beachem (9).
- (e) Hydrogen in solution at low concentration levels results in enhanced dislocation generation and motion.
- (f) The TG fracture mechanism is related to hydrogen enhanced plasticity along 111 planes in front of the crack tip.

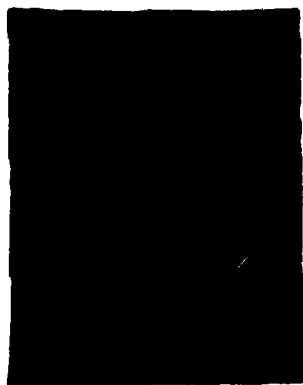
V. Acknowledgements

This work was supported by the Office of Naval Research Contract N00014-75-C-1012 and by the National Science Foundation Grant DMR 77-09808. We would like to acknowledge the support of the HVEM facility at the Argonne National Laboratory and to particularly thank Mr. A. Philippides and Mr. E. Ryan for their assistance with the HVEM experiments.

References

1. G. C. Smith, pp. 485-511 in Hydrogen in Metals, I. M. Bernstein and A. W. Thompson, eds.; ASM, Metals Park, 1974.
2. T. Matsumoto and H. K. Birnbaum, Hydrogen in Metals, Proceedings of the Second J.I.M. International Symposium, Transactions of the Japan Institute of Metals Supplement, 21 (1980) 493.
3. A. M. Windle and A. C. Smith, Journal of Material Science, 4 (1970) 136.

4. M. H. Kamdar, Paper 3D10 in Proceedings of the Second International Congress on Hydrogen in Metals; Pergamon, Oxford, 1977.
5. B. A. Wilcox and G. C. Smith, Acta Metallurgica, 12 (1964) 371.
6. R. H. Stulen, Hydrogen in Metals, Proceedings of the Second J.I.M. International Symposium, Transactions of the Japan Institute of Metals Supplement, 21 (1980) 501.
7. S. P. Lynch, Scripta Metallurgica, 13 (1979) 1051.
8. H. Matsui, H. Kimura and S. Moriya, Materials Science and Engineering, 40 (1979) 207; 217.
9. C. D. Beachem, Metallurgical Transactions, 3 (1972) 437.



(1a) 10 μ



(1b) 1 μ



(1c) 50 μ



(1d) 3 μ



(1e) 10 μ



(1f) 10 μ



(1g) 10 μ ———



(1h) 4 μ ———

- Fig. 1 - Characteristic transgranular fracture surface features.**
- (1a) - $\{111\}$ fracture surface showing intersecting $\{111\}$ slip plane traces. Fracture in H_2 gas; single crystal.
 - (1b) - Same as (a) at high magnification. No evidence is found for microvoid formation.
 - (1c) - Hillocks formed by intersecting $\{211\}$ slip planes.
 - (1d) - Same as (c) at high magnification.
 - (1e) - Secondary cracking on transgranular fracture surface formed by stressing in H_2 gas.
 - (1f) - Stepped transgranular fracture surface formed in polycrystalline specimen stressed in H_2 gas. The surface is of the "quasicleavage" type showing "cleavage" steps and apparent crack arrest markings.
 - (1g) - "Quasicleavage" fracture surface formed in polycrystalline specimen stressed in H_2 gas.
 - (1h) - Same as (g) at higher magnification.



(2a) 20 μ ———



(2b) 20 μ ———

- Fig. 2 - Characteristic intergranular fracture surface features. Similar features are observed for specimens fractured in H_2 gas or containing solute hydrogen.**
- (2a) - Slip line traces.
 - (2b) - Localized regions of high ductility.



(3a) 200 μ 



(3b) 100 μ 



(3c) 200 μ 



(3d) 100 μ 

Fig. 3 - In-situ SEM micrographs of propagating cracks.

- (3a) - Intergranular fracture in specimen containing solute hydrogen. Micrograph shows crack nucleation in front of the main crack; large COD.
- (3b) - Intergranular fracture showing crack nucleation in front of the main crack and the large slip zone in front of the crack.
- (3c) - Intergranular fracture showing large COD and large shear displacements along adjacent grain boundaries.
- (3d) - Transgranular fracture showing large COD and the slip zone in front of the crack.



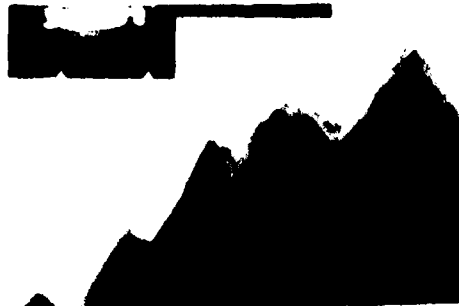
(4a) 10 μ 



(4b) 10 μ 



(4c) 10 μ



(4d) 2 μ



(4e) 0.5 μ



(4f) 0.5 μ



(4g)
2 μ

Fig. 4 - HVEM micrographs of propogating cracks.

- (4a) - Noncrystallographic fracture for specimens stressed in Vacuum.
- (4b) - Same as (a). Crack tip region showing "hole" formation in front of the main crack.
- (4c) - Crystallographic fracture for specimens stressed in H_2 gas. Fracture surfaces are the $\{111\}$.
- (4d) - Same as (c). The thinned regions along the fracture surfaces result from slip along the $\{111\}$ causing the sawtooth appearance.
- (4e) - Dislocation structure in front of a crack tip formed in H_2 gas showing intense slip in front of the crack.

- (4f) - Same as (e). Region further along in front of the crack.
 (4g) - High dislocation densities localized along the fracture surfaces of specimens fractured in H_2 gas.

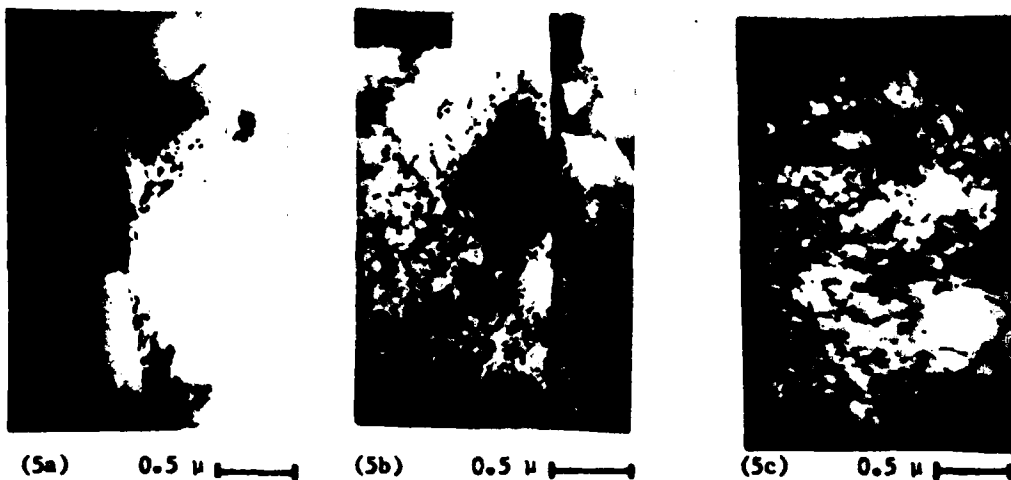


Fig. 5 - HVEM micrographs of dislocation structures formed during insitu deformation.

- (5a) - Specimen stressed in vacuum.
 (5b) - Same area as (5a) after the introduction of H_2 gas while the specimen is held under stress at constant displacement.
 (5c) - Dislocation structure resulting from the introduction of H_2 gas after the specimen was stressed in vacuum. Prior to the introduction of H_2 gas no dislocations were visible in this region.

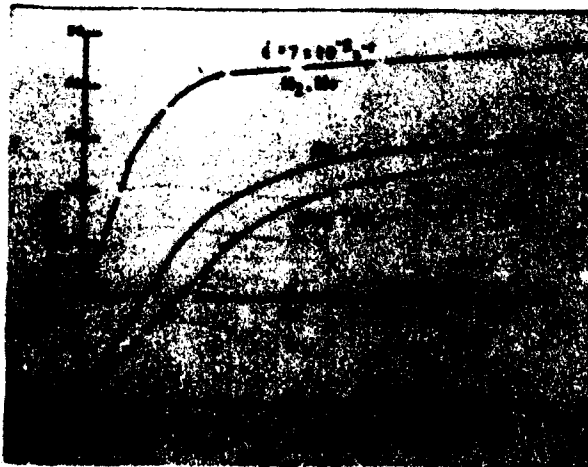


Fig. 6 - Initial portions of the stress strain curves for specimens tested in He or H_2 gas environments at "high" and "low" strain rates.

Unclassified
Security Classification

AD-A094 271

DOCUMENT CONTROL DATA - R & D

(Security classification of title, body of abstract and indexing annotation must be entered when the overall report is classified)

1. ORIGINATING ACTIVITY (Corporate author) <i>University of Illinois Dept. of Metallurgy & Mining</i>		2a. REPORT SECURITY CLASSIFICATION <i>Unclassified</i>	
3. REPORT TITLE <i>Hydrogen Effects in Nickel - Embrittlement or Enhanced Ductility</i>		2b. GROUP	
4. DESCRIPTIVE NOTES (Type of report and, inclusive dates) <i>Technical Report</i>			
5. AUTHOR(S) (First name, middle initial, last name) <i>J. Eastman, T. Matsumoto, M. Harita, F. Neubauer and H.K. Bunbaum</i>			
6. REPORT DATE <i>Nov. 1980</i>		7a. TOTAL NO. OF PAGES <i>12</i>	7b. NO. OF REFS <i>9</i>
8a. CONTRACT OR GRANT NO. <i>N 00014-75-C-1012</i>		9a. ORIGINATOR'S REPORT NUMBER(S)	
b. PROJECT NO.		9b. OTHER REPORT NO(S) (Any other numbers that may be assigned this report)	
c.			
d.			
10. DISTRIBUTION STATEMENT <i>This document is unclassified. Reproduction and distribution for any purpose of the U.S. Government is permitted</i>			
11. SUPPLEMENTARY NOTES		12. SPONSORING MILITARY ACTIVITY <i>Office of Naval Research</i>	
13. ABSTRACT <i>Use abstract from pages</i>			

Unclassified

Security Classification

14 KEY WORDS	LINK A		LINK B		LINK C	
	ROLE	WT	ROLE	WT	ROLE	WT
Hydrogen Embrittlement Nickel Fracture Plastic Deformation						

DD FORM 1473 (BACK)
1 NOV 65

5110-107-02-00-1

Unclassified
Security Classification

4-31400

**DAT
FILM**